Full simulations of the apertureless scanning near field optical microscopy signal: achievable resolution and contrast

R. Esteban[1,2*],**R. Vogelgesang**[1],**K,Kern**[1,3]

[1] *Max Planck Institute für Festkörperforschung, 70569 Stuttgart, Germany*
[2]*Institut d'Optique Graduate School, 91127 Palaiseau, France*
[3]*Institut de Physique des Nanostructures, Ecole Polytechnique Fédérale de Lausanne, CH-1015 Lausanne, Switzerland*
ruben.esteban@institutoptique.fr

Abstract: We simulate apertureless near-field optical imaging and obtain phase and amplitude scans of structured substrates for elastic scattering. The solution of the three-dimensional Maxwell equations does not involve approximations and we include large tips and substrates, strong interaction, interferometric detection and demodulation at higher harmonics. Such modeling represents a significant step towards quantitative simulations and offers the attractive possibility to study the individual influence of each relevant experimental parameter. We typically obtain highly localized signatures of the interaction of the tip with gold inclusions, superposed on a slowly varying background signal. The relative importance of both contributions and the achievable lateral resolution are strongly dependent on the geometry and scanning conditions. The simulations show sensitivity mostly to the first nanometers of the sample and underline the importance of scanning near the sample and being careful with mechanical anharmonicities on the tip oscillation. They also help to determine the influence of oscillation amplitude and demodulation harmonic.

OCIS codes: (180.4243) Near-field microscopy; (290.5870) Scattering, Rayleigh; (999.9999) Field enhancement.

References and links

1. D. W. Pohl, W. Denk, and M. Lanz, "Optical Stethoscopy: Image Recording with Resolution $\lambda/20$," Appl. Phys. Lett. **44**, 651–653 (1984).
2. S. Hell, "Toward fluorescence nanoscopy," Nat. Biotech. **21**, 1347–1355 (2003).
3. M. J. Rust, M. Bates, and X. Zhuang, "Sub-Diffraction-Limit Imaging by Stochastic Optical Reconstruction Microscopy (STORM)," Nat. Methods **3**, 793–795 (2006).
4. Z. Liu, H. Lee, Y. Xiong, C. Sun, and X. Zhang, "Far-field Optical Hyperlens Magnifying Sub-Diffraction-Limited Objects," Science **315**(5819), 1686 (2007).
5. F. Zenhausern, Y. Martin, and H. K. Wickramasinghe, "Scanning Interferometric Apertureless Microscopy: Optical Imaging at 10 Angstrom Resolution," Science **269**, 1083–1085 (1995).
6. B. Knoll and F. Keilmann, "Near-Field Probing of Vibrational Absorption for Chemical Microscopy," Nature **399**, 134–137 (1999).
7. T. Taubner, R. Hillenbrand, and F. Keilmann, "Performance of Visible and Mid-Infrared Scattering-Type Near-Field Optical Microscopes," J. Microsc. **210**, 311–314 (2003).

#104783 - $15.00 USD Received 1 Dec 2008; revised 14 Dec 2008; accepted 15 Dec 2008; published 6 Feb 2009

8. A. Bek, R. Vogelgesang, and K. Kern, "Apertureless Scanning Near-field Optical Microscope with sub-10nm Resolution," Rev. Sci. Instrum. **77**, 043703 (2006).
9. A. Hartschuh, E. J. Sanchez, X. S. Xie, and L. Novotny, "High-Resolution Near-Field Raman Microscopy of Single-Walled Carbon Nanotubes," Phys. Rev. Lett. **90**, 095503 (2003).
10. N. Ocelic and R. Hillenbrand, "Subwavelength-Scale Tailoring of Surface Phonon Polaritons by Focused Ion-Beam Implantation," Nat. Materials **3**, 606–609 (2004).
11. Z. Ma, J. M. Gerton, L. A. Wade, and S. R. Quake, "Fluorescence Near-Field Microscopy of DNA at sub-10nm Resolution," Phys. Rev. Lett. **97**, 260801 (2006).
12. J. T. Krug II, E. J. Sánchez, and X. S. Xie, "Design of Near-Field Optical Probes with Optimal Field Enhancement by Finite Difference Time Domain Electromagnetic Simulation," J. Chem. Phys. **116**, 10895–10901 (2002).
13. K. B. Crozier, A. Sundaramurthy, G. S. Kino, and C. F. Quate, "Optical Antennas: Resonators for Local Field Enhancement," J. Appl. Phys. **94**, 4632–4642 (2003).
14. R. Esteban, R. Vogelgesang, and K. Kern, "Simulation of Optical Near and Far Fields of Dielectric Apertureless Scanning Probes," Nanotechnology **17**, 475–482 (2006).
15. M. Micic, N. Klymyshyn, Y. D. Suh, and H. P. Lu, "Finite Element Method Simulation of the Field Distribution for AFM Tip-Enhanced Surface-Enhanced Raman Scanning Microscopy," J. Phys. Chem. B **107**, 1574–1584 (2003).
16. J. A. Porto, P. Johansson, S. P. Apell, and T. López-Ríos, "Resonance Shift Effects in Apertureless Scanning Near-Field Optical Microscopy," Phys. Rev. B **67**, 085409 (2003).
17. J. Renger, S. Grafström, L. M. Eng, and V. Deckert, "Evanescent Wave Scattering and Local Electric Field Enhancement at Ellipsoidal Silver Particles in the Vicinity of a Glass Surface." J. Opt. Soc. Am. A **21**, 1362–1367 (2004).
18. R. M. Roth, N. C. Panoiu, M. M. Adams, R. M. Osgood, Jr., C. C. Neacsu, and M. B. Raschke, "Resonant-plasmon field enhancement from asymmetrically illuminated conical metallic-probe tips," Opt. Express **14**, 2921–2931 (2006).
19. R. Esteban, R. Vogelgesang, and K. Kern, "Tip-Substrate Interaction in Optical Near Field Microscopy," Phys. Rev. B **75**, 195410 (2007).
20. M. Labardi, S. Patanè, and M. Allegrini, "Artifact-Free Near-Field Optical Imaging by Apertureless Microscopy," Appl. Phys. Lett. **77**, 621–623 (2000).
21. R. Hillenbrand, B. Knoll, and F. Keilmann, "Pure Optical Contrast in Scattering-Type Scanning Nearfield Microscopy," J. Microsc. **202**, 77–83 (2001).
22. J. N. Walford, J. A. Porto, R. Carminati, J.-J. Greffet, P. M. Adam, S. Hudlet, J.-L. Bijeon, A. Stashkevich, and P. Royer, "Influence of Tip Modulation on Image Formation in Scanning Near-Field optical Microscopy," J. Appl. Phys. **89**, 5159–5169 (2001).
23. R. Hillenbrand, F. Keilmann, P. Hanarp, D. S. Sutherland, and J. Aizpurua, "Coherent Imaging of Nanoscale Plasmon Patterns with a Carbon Nanotube Optical Probe," Appl. Phys. Lett. **83**, 368–370 (2003).
24. R. Bachelot, G. Lerondel, S. Blaize, S. Aubert, A. Bruyant, and P. Royer, "Probing Photonic and Optoelectronic Structures by Apertureless Scanning Near-Field Optical Microscopy." Microsc. Res. Tech. **64**, 441–452 (2004).
25. L. Stebounova, F. Chen, J. Bain, T. E. Schlesinger, S. Ip, and G. C. Walker, "Field Localization in Very Small Aperture Lasers Studied by Apertureless Near-Field Microscopy," Appl. Opt. **45**, 6192–6197 (2006).
26. R. Esteban, R. Vogelgesang, J. Dorfmüller, A. Dmitriev, C. Rockstuhl, C. Etrich, and K. Kern, "Direct Near-Field Optical Imaging of Higher Order Plasmonic Resonances," Nano Lett **8**, 3155–3159 (2008).
27. C. Girard and A. Dereux, "Optial Spectroscopy of a Surface at the Nanometer Scale: A Theoretical Study in Real Space," Phys. Rev. B **49**, 11344–11351 (1994).
28. M. Xiao and S. Bozhevolnyi, "Imaging with Reflection Near-Field Optical Microscope: Contributions of Middle and Far Fields," Opt. Commun. **130**, 337–347 (1996).
29. R. A. Frazin, D. G. Fischer, and P. S. Carney, "Information Content of the Near Field: Two-Dimensional Samples," J. Opt. Soc. Am. A **21**, 1050–1057 (2004).
30. R. Carminati and J.-J. Greffet, "Influence of Dielectric Contrast and Topography on the Near Field Scattered by an Inhomogenous Surface," J. Opt. Soc. Am. A **12**, 2716–2725 (1995).
31. P. M. Adam, J. L. Bijeon, G. Viardot, and P. Royer, "Analysis of the Influence of the Tip Vibration in the Formation of Images in Apertureless Scanning Near-Field Optical Microscopy," Opt. Commun. **174**, 91–98 (2000).
32. J. Koglin, U. C. Fischer, and H. Fuchs, "Material Contrast in Scanning Near-Field Optical Microscopy at 1-10 Nm Resolution," Phys. Rev. B **55**, 7977–7984 (1997).
33. A. Madrazo, M. Nieto-Vesperinas, and N. García, "Exact Calculation of Maxwell Equations for a Tip-Metallic Interface Configuration:Application to Atomic Resolution by Photon Emission," Phys. Rev. B **53**, 3654–3657 (1996).
34. M. Quinten, "Evanescent Wave Scattering by Aggregates of Clusters - Application to Optical Near-Field Microscopy," App. Phys. B **70**, 579–586 (2000).
35. R. Fikri, T. Grosges, and D. Barchiesi, "Apertureless Scanning Near-Field Optical Microscopy: Numerical Modeling of the Lock-in Detection," Opt. Commun. **232**, 15–23 (2004).
36. C. Hafner, *Post-modern Electromagnetics: Using Intelligent MaXwell Solvers* (John Wiley & Sons Ltd, Chich-

#104783 - $15.00 USD Received 1 Dec 2008; revised 14 Dec 2008; accepted 15 Dec 2008; published 6 Feb 2009

ester, 1999).
37. E. Moreno, D. Erni, C. Hafner, and R. Vahldieck, "Multiple Multipole Method with Automatic Multipole Setting Applied to the Simulation of Surface Plasmons in Metallic Nanostructures," J. Opt. Soc. Am. A **19**, 101–111 (2002).
38. P. B. Johnson and R. W. Christy, "Optical Constants of the Noble Metals," Phys. Rev. B **6**, 4370–4379 (1972).
39. D. E. Aspnes and A. A. Studna, "Dielectric Functions and Optical Parameters of Si, Ge, GaP, GaAs, GaSb, InP, InAs, and InSb from 1.5 to 6.0 eV," Phys. Rev. B **27**, 985–1009 (1983).
40. R. Esteban, "Apertureless SNOM : Realistic Modeling of the Imaging Process and Measurements of Resonant Plasmonic Nanostructures." Ph.D. thesis, EPFL (2007).
41. M. B. Raschke and C. Lienau, "Apertureless Near-Field Optical Microscopy: Tip-Sample Coupling in Elastic Light Scattering," Appl. Phys. Lett. **83**, 5089–5091 (2003).
42. R. Hillenbrand and F. Keilmann, "Complex Optical Constants on a Subwavelength Scale," Phys. Rev. Lett. **85**, 3029–3032 (2000).
43. N. Anderson, P. Anger, A. Hartschuh, and L. Novotny, "Subsurface Raman Imaging with Nanoscale Resolution," Nano Lett. **6**, 744–749 (2006).
44. R. Vogelgesang, R. Esteban, and K. Kern, "Beyond Lock-in Analysis for Volumetric Imaging in Apertureless Scanning Near-Field Optical Microscopy," J. Microsc. **229**, 365–370 (2008).
45. J. L. Bijeon, P. M. Adam, D. Barchiesi, and P. Royer, "Definition of a Simple Resolution Criterion in an Apertureless Scanning Near-Field Optical Microscope (A-SNOM): Contribution of the Tip Vibration and Lock-in Detection," Eur. Phys. J. Appl. Phys. **26**, 45–52 (2004).
46. R. W. Stark and W. M. Heck, "Higher harmonics imaging in tapping-mode atomic-force microscopy," Rev. Sci. Inst. **74**, 5111–5114 (2003).
47. A. Bek, R. Vogelgesang, and K. Kern, "Optical Nonlinearity versus Mechanical Anharmonicity Contrast in Dynamic Mode Apertureless Scanning Nearfield Optical Microscopy," Appl. Phys. Lett. **87**, 163115 (2005).
48. M. Brehm, T. Taubner, R. Hillenbrand, and F. Keilmann, "Infrared Spectroscopic Mapping of Single Nanoparticles and Viruses at Nanoscale Resolution," Nano Lett. **6**, 1307–1310 (2006).
49. F. J. Giessibl, "Forces and frequency shifts in atomic-resolution dynamic-force microscopy," Phys. Rev. B **56**, 16010–16015 (1997).
50. N. A. Burnham, O. P. Behrend, F. Oulevey, G. Gremaud, P.-J. Gallo, D. Gourdon, E. Dupas, A. J. Kulik, H. M. Pollock, and G. A. D. Briggs, "How does a tip tap?" Nanotechnology **8**, 67–75 (1997).
51. T. Taubner, F. Keilmann, and R. Hillenbrand, "Nanoscale-resolved subsurface imaging by scattering-type near-field optical microscopy," Opt. Express **13**, 8893–8899 (2005).
52. B. B. Akhremitchev, S. Pollack, and G. C. Walker, "Apertureless Scanning Near-Field Infrared Microscopy of a Rough Polymeric Surface," Langmuir **17**, 2774–2781 (2001).
53. J. Aizpurua, T. Taubner, F. J. García de Abajo, M. Brehm, and R. Hillenbrand, "Substrate-enhanced infrared near-field spectroscopy," Opt. Express **16**, 1529–1545 (2008).
54. Z. H. Kim, B. Liu, and S. R. Leone, "Nanometer-Scale Optical Imaging of Epitaxially Grown GaN and InN Islands Using Apertureless Near-Field Microscopy," J. Phys. Chem. B **109**, 8503–8508 (2005).

1. Introduction

Among the techniques developed in recent years to obtain optical lateral resolution beyond the diffraction limit [1, 2, 3, 4] apertureless scanning nearfield optical microscopy (*aSNOM*) is particularly promising [5, 6]. It is fundamentally surface-sensitive and has been shown to give optical information with lateral resolution even below the 10*nm* range [7, 8]. Usually, a sample is externally excited, and the radiation scattered by a probing tip carries local information about the volume in the proximity of its apex. Experimental work shows clear images for a wide array of sample types [9, 10, 11].

A fundamental challenge to obtain, optimize and interpret experimental images is the dependence of the measured signal on various experimental parameters, not all of which are necessarily known or well controlled. In this context, numerical simulations offer an opportunity to define and change relevant conditions at will and are useful for a better understanding of the phenomena involved. Solving the Maxwell equations under conditions which are found in many experiments is, however, challenging: the substrate can be complex, the size and shape of the tip can influence the results [12, 13, 14], strong interaction [15, 16, 17, 18, 19] between tip and sample is common and while the tip and the substrate can be large relative to the excitation wavelength, other parameters of importance such as the tip-substrate distance can be

#104783 - $15.00 USD Received 1 Dec 2008; revised 14 Dec 2008; accepted 15 Dec 2008; published 6 Feb 2009

in the nanometer range. Further, the way in which the signal is detected has been observed to be critical; very significantly for elastic information, demodulating the signal at the higher harmonic of the frequency of oscillation [20, 21] can enhance the contributions described by fast spatial variation, i.e. those enabling high resolution [22]. Interferometric detection allows to obtain both phase and amplitude information.

Much of the theoretical understanding of *aSNOM* has been gained by reasoning with one of two simplifying assumptions. The first considers a passive – or weakly perturbing – tip that serves to scatter the fields present in the sample [23, 24, 25, 26]. We note that as far as the effect of the tip on the field distribution is not critical, relevant results can also be drawn from work not specific to *aSNOM* discussing the spatial behavior of near fields in general. The localized nature of the near fields, which allows to obtain high lateral resolution [27], the convenience to scan near the sample [28, 29], the influence of optical and topographical contrast [30] and the effect of higher harmonic demodulation [31, 22] have all been studied. The second alternative assumes a tip that strongly interacts with a flat substrate. Under such conditions, the signal is understood as probing the strength of the interaction, and consequently the dielectric constant of the surface [32, 6].

For interpreting measurements, however, one would desire to understand in detail the origin of the optical signal in a general scenario, which is not restricted to one of the limiting cases discussed above; a tip scans a sample of complex topography and dielectric properties, and can interact more or less strongly with the sample according to position. First studies have already started to tackle some of the questions of interest [33, 34, 35], but simulating the conditions of typical experiments is still highly challenging. Here, we aim to improve the understanding of *aSNOM* by studying in detail the process of image formation for models close to experiments under general conditions. In particular, we solve for elastic scattering the three-dimensional Maxwell equations simultaneously including patterned samples, elongated tips, strong tip-sample interaction, interferometric detection and higher harmonic demodulation. We use our simulations to discuss the need of including long tips for realistic simulations and to quantitatively study the dependance on relevant experimental parameters of key aspects of *aSNOM* imaging: signal strength, resolution, background suppression and contrast between areas of different physical properties.

2. Model

For the simulation, we use the MaX-1 software package, a program based on the multiple multipole method [36, 37]. It uses multipole and other field distributions that verify the bulk Maxwell equations and serve as expansion sets for the resulting electromagnetic field distributions. The expansion coefficients are determined by a minimization of the error in the boundary conditions. In our case, we keep the average error smaller than 0.5 percent and verify that increasing the number of free parameters in the expansions by ~ 25 or ~ 50 percent does not significantly affect the discussed results.

Figure 1 sketches the simulated geometry. For the environment we assume vacuum ($\varepsilon_0 = 1.0$). Unless mentioned otherwise, we concentrate on a $500nm$ long conical tip of 10 degree opening angle, capped with two hemispheres. The tip apex has radius $R = 10nm$. The tip is made of silicon ($\varepsilon_{Si} = 17.76 + 0.508i$ [39]) and it oscillates at an angular frequency Ω along the z axis, simulating the motion of a non-contact mode atomic force probe along this axis.

The substrate is a spherical gold inclusion of $10nm$ radius at a small distance $d^{(i)}$ to the surface of a much larger glass sphere, of $2\mu m$ diameter ($\varepsilon_{Au} = -3.95 + 2.58i$ [38], $\varepsilon_{glass} = 2.1$). The line joining the centers of both spheres is parallel to the tip axis. The point of the glass-vacuum interface exactly above the center of the inclusion is the origin of the coordinate system used to facilitate the discussion. The small gold inclusion facilitates illustration of the excel-

#104783 - $15.00 USD Received 1 Dec 2008; revised 14 Dec 2008; accepted 15 Dec 2008; published 6 Feb 2009

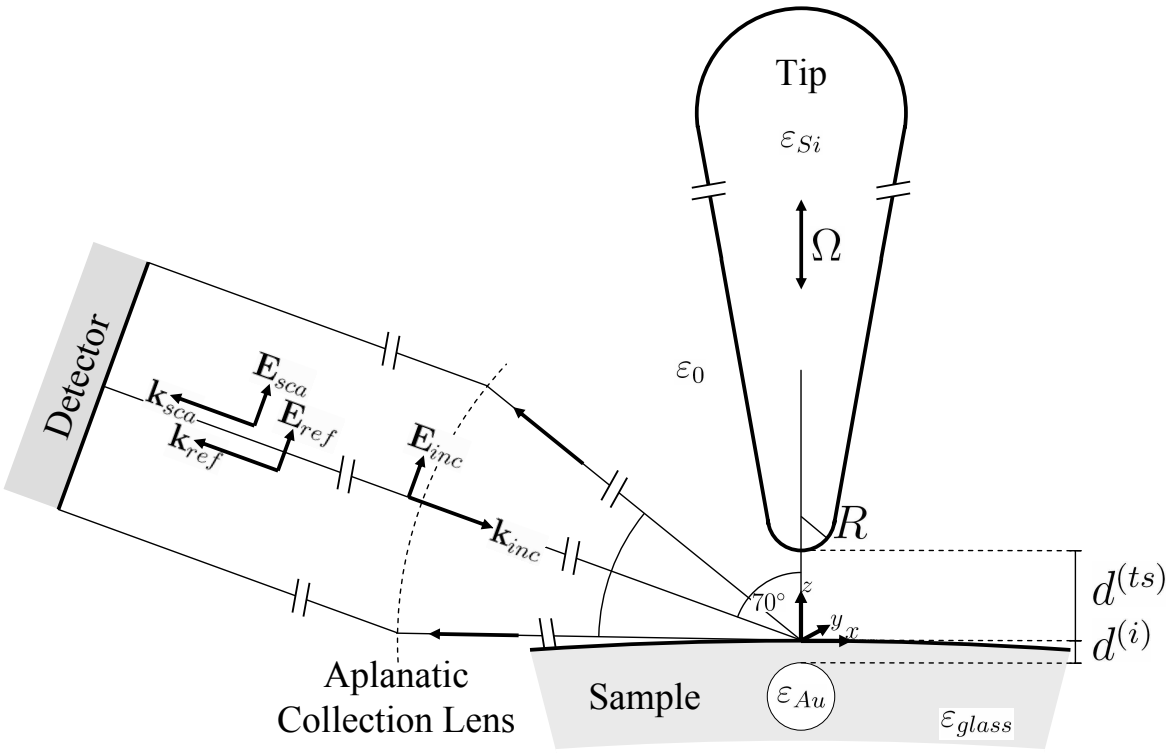

Fig. 1. Illustration of the geometry used. The illumination is modeled as a planar wave, and for collection an aplanatic lens situated at 1mm distance is considered. A reference beam is used for amplified, interferometric detection. The upper point of the glass substrate serves as the origin of the coordinate system.

lent lateral resolution that is one of the main justifications for *aSNOM*. Changing the depth of the inclusion $d^{(i)}$ also opens a natural way to study how far the tip probes into the substrate. The radius of the glass substrate is large enough to be locally almost flat at the region of interest. We used a curved substrate to avoid numerical convergence difficulties when evaluating the scattered fields at the detector. Both the size of the large substrate sphere and of the tip length, comparable to the wavelength, represents a reasonable compromise between numerical requirements and the desire to resemble typical experimental conditions. We have discussed previously the influence of changing the tip length and substrate radius [19].

A p-polarized planar wave of wavelength $\sim 514.5nm$, propagation vector $\mathbf{k}$ and electric field $\mathbf{E}$ illuminates the sample at an incident angle of 70° with respect to the tip axis. We calculate the fields from the large sphere in isolation and from the complete tip-substrate system; we subtract the former from the latter to concentrate on the contribution from the tip and the inclusion. Simulating focused illumination is useful to avoid scattering from the top cap of long tips [19]. However, the radius of the illumination focus for typical *aSNOM* experiments under lateral illumination can easily be significantly bigger than the tip length in this paper, so that the gaussian illumination is similar to a planar wave in the region of interest. We thus consider the simple planar wave illumination to be sufficient for the tip lengths and purposes of the present paper.

A lens of numerical aperture ~ 0.342 situated at $1mm$ distance in the back scattering direction collects the scattered fields. We ignore any effects of further optical elements or propagation on

#104783 - $15.00 USD Received 1 Dec 2008; revised 14 Dec 2008; accepted 15 Dec 2008; published 6 Feb 2009

the collected fields until they impinge normally on a photodetector, but we do include interferometric mixing with a collinear reference planar wave polarized in the *xz* plane (p polarized). The lens is an idealized aplanat, that is, a non-absorbing, non-reflecting converter of a spherical waves centered on $x = z = 0$ into a beam of planar phase front propagating towards the photodetector.

Further, we consider the effect of a dual-phase lock-in amplifier operating at angular frequency $n\Omega$, which subsequently gives the amplitude and phase of the n-th harmonic of the signal H_n generated by the photodetector. Assuming the reference beam used for interferometric detection much stronger than the fields scattered by the tip and sample, we write [40]

$$H_n \propto \frac{e^{i\phi_{li}}}{2T} \int_0^T e^{in\Omega t} \int_{S_{det}} \mathscr{E}^*(\mathbf{r}, x, d^{(ts)}(t)) d^2 r dt \tag{1}$$

$\mathscr{E}^*(\mathbf{r}, x, d^{(ts)}(t))$ describes the magnitude and phase of the complex conjugate of the scattered electric field amplitude at the photodetector, for the p-polarized component. The presence or not of complex conjugates in the terms of Eq. (1) depends on the exact experimental implementation [40] but is of little importance here. $\mathscr{E}^*$ is a function of the area element location $\mathbf{r}$ and tip position at a given time$(x, d^{(ts)}(t))$. If not mentioned otherwise, the tip oscillates along z as $d^{(ts)}(t) = d_{min} + A[1 + \cos(\Omega t)]$, where A is the amplitude of the oscillation and d_{min} the minimum tip-substrate distance, constant during a given scan. S_{det} is the area of the detector where the fields are non-zero, as defined by the numerical aperture of the lens, and ϕ_{li} allows to consider the internal phase of the lock-in amplifier or the phase of the reference beam, which only enter a constant offset to the phase of the signal. To simulate a scan along x, we evaluate Eq. (1) by varying $d^{(ts)}$ for each x position of the tip. That is, we consider the tip being displaced over a fixed substrate rather than the sample under a horizontally fixed tip, which may be advantageous in experiments using focussed beam excitation [8]. For the plane wave excitation assumed here, the difference is a simple phase shift proportional to the tip position. The units of the obtained amplitude signal are arbitrary, as they depend on the reference signal power and photodetector sensitivity, but they are kept constant throughout the manuscript.

Generally, the simulated $|H_n|$ scans exhibit a component slowly varying across the inclusion on a scale significantly larger than the inclusion and a peak-like signature confined to small tip-inclusion distances. For the purpose of this paper, we refer to the former as background, whereas the latter we associate with signal due to tip-inclusion interactions. We discuss the images in terms of the peak height (absolute and relative to the background level) and the full width half maximum $FWHM$ of the central peak. Thus, to calculate the $FWHM$ we first subtract from $|H_n|$ an estimation of the background, given by the linear interpolation between the values at $x = -39nm$ and $x = 39nm$.

3. Results

3.1. General characteristics of the obtained signal

Figure 2(a) illustrates how the tip interacts with the substrate. Strong near fields appear between the tip and the closely situated gold inclusion, significantly more intense than between the tip and the glass. For more qualitative information, the insert shows the normalized value of the near field maximum in the proximity of the apex for separation $d_{min} = 1nm$ and different tip positions along x. The near fields are significantly stronger when the tip is close to the gold inclusion than to the glass substrate, as expected [41]. However, also in the insert, no corresponding far field signature appears clearly in the plotted behavior of $|\int_{S_{det}} \mathscr{E}(\mathbf{r}, x, d^{(ts)} = 1nm) d^2 r|$ before demodulation.

A representative example of one-dimensional scans ($d_{min} = 1nm$, $d^{(i)} = 1nm$, and $A = 10nm$)

#104783 - $15.00 USD Received 1 Dec 2008; revised 14 Dec 2008; accepted 15 Dec 2008; published 6 Feb 2009

(a) (b)

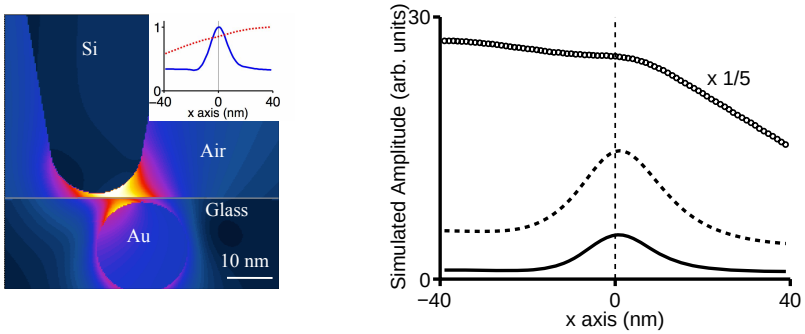

(c)

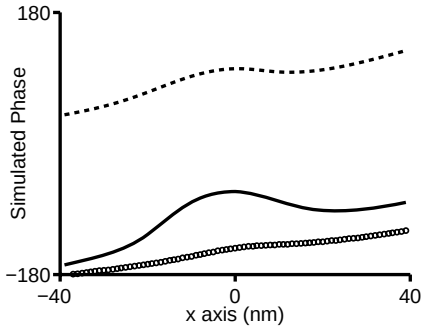

Fig. 2. (a) Example of the field distribution of the average scattered electric field in the proximity of the tip apex, for 500nm long tip and $d^{(ts)} = d^{(i)} = 1nm$. The colors indicate values between 0 and 15, where the excitation field strength is 1. The insert indicates the normalized value of the near field maximum in the proximity of the apex (continuous blue) and the normalized amplitude of the interferometric term of the signal before demodulation (dashed red), for 1nm distance to the substrate. (b,c) Examples of the obtained amplitude (b) and phase (c) for one-dimensional scans of the samples, for the first (circles), second (dashed) and third (continuous) harmonics, the geometry described in (a), $d_{min} = 1nm$ and $A = 10nm$. For better visibility, the first harmonic amplitude is scaled by 1/5.

#104783 - $15.00 USD Received 1 Dec 2008; revised 14 Dec 2008; accepted 15 Dec 2008; published 6 Feb 2009

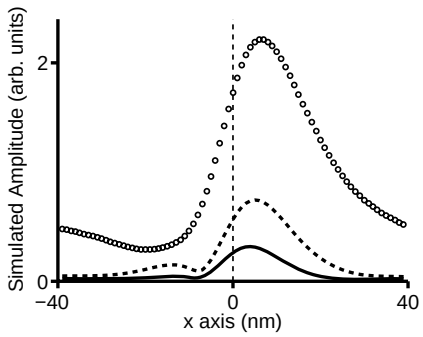

Fig. 3. Amplitude of the signal for one-dimensional scans of the sample when a small spherical tip is considered, for the first (circles), second (dashed) and third (continuous) harmonics. $d^{(i)} = 1nm$, $d_{min} = 1nm$ and $A = 10nm$. The radius of the spherical tip is $10nm$.

at the first three harmonics is plotted in Fig. 2(b,c). Not plotted, the continuous component ($|H_0|$) gives a signal ~ 25 times larger than the first harmonic and similar in shape to the signal before demodulation $|\int_{S_{det}} \mathscr{E}(\mathbf{r}, x, d^{(ts)} = 1nm) d^2r|$ shown in the insert of Fig. 2(a). Looking at the amplitude of the detected signal, a clearly stronger signal near the inclusion appears at the second and third harmonics, but not in the first. The signal is stronger for the lower harmonics, but the contrast between the maximum and the signal for $x \gg R$ diminishes. The width of the maxima is much smaller than the wavelength, which confirms the possibility of lateral resolution much below the diffraction limit. In Fig. 2(b), the $FWHM$ of the second and third harmonic is $\sim 21nm$ and $\sim 17nm$, respectively.

Our model is able to simulate both amplitude and phase information of the demodulated complex optical field strength [42] as is often recorded in experimental work. Here we note that we have found the detected phase (Fig. 2(c)) at second and third harmonic demodulation to also reveal local extrema near $x = 0$. As for the amplitude, the phase signature appears more pronounced in the third harmonic than the second. Notice that in accordance to our discussion of Eq. (1), the sign of the phase –and thus the character of the extrema as minima or maxima– depends on the particular experimental implementation. For the remainder of this manuscript we concentrate on amplitude signals exclusively.

3.2. Tip length and inclusion depth

Theoretical *aSNOM* studies often model small tips, and we briefly consider in Fig. 3 consequences of such an assumption for conditions otherwise identical to Fig. 2(b). For a tip modeled as a sphere of $10nm$ radius (equal to the apex radius of the long tips), the signal is considerably weaker in Fig. 3, an effect especially pronounced for the first harmonic, where the strong scattering from the bulk of long tips is more relevant [19]. The central maximum dominates the obtained signal even for the first harmonic and is *not* situated at $x = 0$, i.e., the asymmetry introduced by the illumination has a measurable influence. Notice that in the long tip case (Fig. 2(b)), the second and third harmonic signal were much more symmetric. The maxima are also narrower for the small than for the long tip, with the $FWHM$ at the third harmonic $\sim 15 - 20$ percent smaller than before.

Back to the long tip case, we consider in Fig. 4 the influence of the depth of the inclusion, $d^{(i)}$ [41, 43]. When $d^{(i)}$ is increased, the amplitude of the signal remains approximately constant for $|x| \gg R$ but rapidly diminishes at the central maximum. For $d^{(i)} = 5nm$, the maximum peak signal after substracting the background is approximately three times weaker than for $1nm$. The

#104783 - $15.00 USD Received 1 Dec 2008; revised 14 Dec 2008; accepted 15 Dec 2008; published 6 Feb 2009

(a)

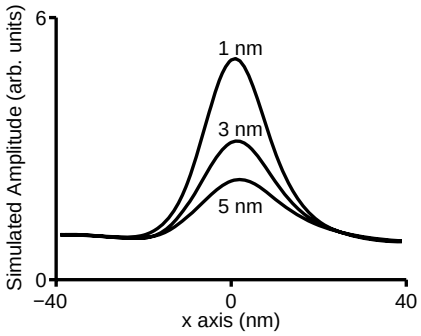

Fig. 4. Influence of the depth of the inclusion, for the third harmonic, on the amplitude of the signal for 1-dimensional scans. 500nm long tip, oscillation amplitude 10nm and $d_{min} = 1nm$ are considered.

(a) (b)

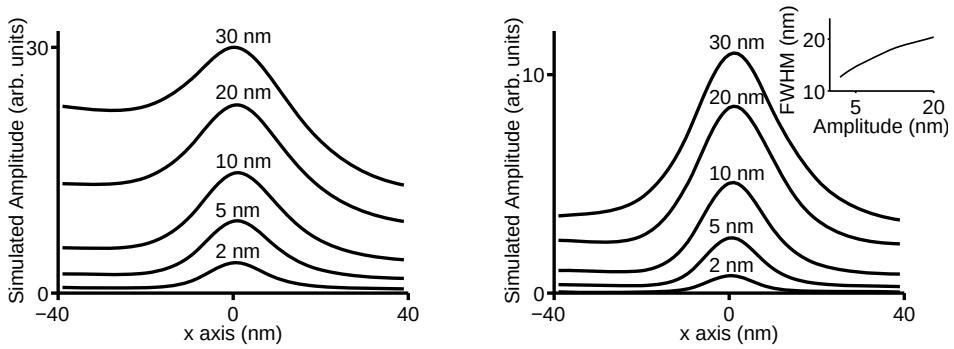

Fig. 5. Influence of the oscillation amplitude on the obtained signal amplitude for the second (a) and third (b) harmonics using 500nm long tips. $d^{(i)} = 1nm$ and $d_{min} = 1nm$. The insert in (b) shows the influence of the oscillation amplitude on the $FWHM$ of the central maximum.

$FWHM$ increases for the larger values of $d^{(i)}$, ~ 17 and $\sim 21nm$ for 1 and 5nm, respectively.

3.3. Scanning parameters

We consider next the influence of the scanning parameters on the resulting scans, starting with the oscillation amplitude A. A Taylor expansion of the signal with respect to z demonstrates that, in the *infinitesimal* amplitude case, the amplitude of the n-th harmonic signal is proportional to the n-th power of the oscillation amplitude [44]. For the second harmonic central maximum and amplitudes varying from 2nm up to values on the order of the apex radius, Fig. 5(a) shows a dependence weaker than quadratic but still important. For much larger values the main effect is a shift of the whole curve towards larger signal, diminishing the contrast between the sig-

#104783 - $15.00 USD Received 1 Dec 2008; revised 14 Dec 2008; accepted 15 Dec 2008; published 6 Feb 2009

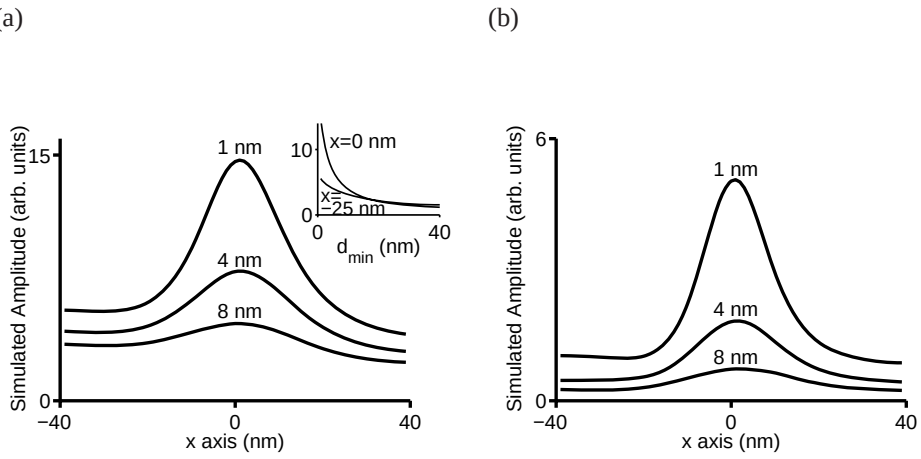

Fig. 6. Influence of d_{min} on the signal amplitude for 1-dimensional scans using 500nm long tips at the second (a) and third (b) harmonics. $d^{(i)} = 1nm$ and the oscillation amplitude is 10nm. The insert in (a) shows the dependence of the signal on d_{min} for $x = 0$ and $x = -25nm$.

nal at the maximum and at values of $|x| \gg R$. A similar trend characterizes the third harmonic (Fig. 5(b)). The main difference in comparison to the second harmonic is that values of oscillation amplitudes as large as three times the apex radius still result in a clear central maximum. The insert demonstrates that increasing the amplitude also affects the $FWHM$ [22, 45]. In our case, it is ~ 60 percent larger for $A = 20nm$ than for $2nm$.

Figure 6 shows, for the second (a) and third (b) harmonic, the influence of changing the minimum distance between tip and substrate d_{min}. Increasing d_{min} on the order of half the apex radius strongly reduces the signal level, most significantly at the maximum. To further illustrate this point, the insert in Fig. 6(a) shows the evolution of the second harmonic signal for a continuous change in d_{min}, for the tip over the inclusion ($x = 0$) and relatively far away ($x = -25nm$). Values $-39nm > x > -25nm$ result in similar traces, indicating that the influence of the inclusion in this range is small. The signal increase for short d_{min} is especially significant when the tip interacts strongly with the inclusion, but it is also present for $x = -25nm$, where the tip mostly interacts with the bare glass substrate. Increasing d_{min} also increases the $FWHM$ (In Fig. 6 (a), from $FWHM \sim 21nm$ at $d_{min} = 1nm$ to $FWHM \sim 25nm$ at $d_{min} = 4nm$).

Up to now, a perfect sinusoidal movement was assumed to describe the tip oscillation. Figure 7 considers the imaging process for a tip movement along z according to $d^{(ts)} = d_{min} + A[1 + b + \cos(\Omega t) + b\cos(3\Omega t)]$, where b is a parameter used to change the deviation from a perfectly harmonic motion. Already for a value of b of 1 percent, the change on the third harmonic signal, in particular for $|x| \gg R$, is not negligible. For a value of b close to 10 percent the change is dramatic, with a much less clear central maximum. Notice that a large signal distortion of the signal could ensue if the strength of the anharmonicity changes during the scan. Such effects are of mechanical [46, 47, 44], and not optical, origin, and are generally undesired for *aSNOM* measurements.

4. Discussion and conclusions

Using patterned substrates, we have been able to simulate amplitude and phase images after higher harmonic demodulation. Demonstrating that phase images can be simulated is relevant

#104783 - $15.00 USD Received 1 Dec 2008; revised 14 Dec 2008; accepted 15 Dec 2008; published 6 Feb 2009

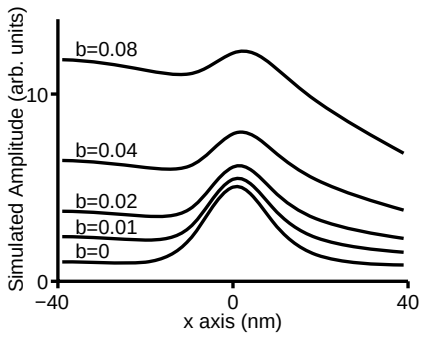

Fig. 7. Influence on 1-dimensional scans of the presence of anharmonicities (described by b) in the movement of a 500nm long tip. The traces correspond to the amplitude of the third harmonic signal, for $d^{(i)} = 1nm$, $d_{min} = 1nm$ and $10nm$ oscillation amplitude.

for *aSNOM* studies in which the phase detected at the lock-in amplifier gives additional information about the sample [10, 48]. As in most *aSNOM* studies, however, the emphasis here is on the amplitude of the final signal.

The choice of tip material serves to illustrate the possibility of *aSNOM* imaging with silicon tips, which can be very sharp. Indeed, commercial tips of apex radius $< 10nm$ are readily available. As far as the tip-substrate interaction is strong enough for discrimination of the resulting signal to be possible, we expect the tip material to affect the signal strength but be of little qualitatively significance to the general behavior. Only for sharp resonances significant spectral shifts could appear as the tip moves close to the substrate [16], modify the appearance of the simulated images, and complicate their interpretation.

Before demodulation, no clear signatures from the inclusion appear. In contrast, the typical signal after higher harmonic demodulation can be conceptually seen as a narrow maximum appearing when the tip is close to the inclusion, riding on a smooth background signal. It seems intuitive to associate the peak with a stronger tip-substrate interaction (continuous line in the insert in Fig. 2(a)). If extended to more complex scenarios, a direct connection may be drawn between the demodulated signal and the interaction strength.

The $FWHM$ is closely related to the point spread function of conventional resolution studies and a small value is a strong indicator of good lateral resolution. We find that a $FWHM$ as low as $\sim 12.5nm$ is possible at the third harmonic for small oscillation amplitude, less than $\lambda/40$ and comparable with both the tip and sphere radius. For comparison, a *topography* image of a 10 *nm* radius hemisphere scanned by an AFM tip with $10nm$ apex radius results in $FWHM$ more than twice larger. Notice that both the structure size and the tip apex radius – identical here – are relevant length scales, even if for simplicity we sometimes only refer to the latter.

The images are clearly dependent on the scanning conditions. Close proximity between the tip and the inclusion is convenient for strong interaction and small $FWHM$. A perfect sinusoidal movement of the tip is also advantageous for experiments, at least as long as the set-up is not capable of separating optical and mechanical contributions [44]. However, both desires are not completely independent in a realistic experiment: strong tip-substrate contact as a consequence of an attempt to decrease d_{min} risks introducing anharmonicities in the tip movement and also fast wear of the tip apex during scanning [47, 44].

It does not seem possible to give an optimal oscillation amplitude and demodulation harmonic valid for all experimental conditions. A small amplitude and high harmonic reduces the $FWHM$ and results in clearer maxima, but it also considerably diminishes the signal level. Too soft a cantilever with too small an amplitude can also result in jump-to-contact, that is, un-

#104783 - $15.00 USD Received 1 Dec 2008; revised 14 Dec 2008; accepted 15 Dec 2008; published 6 Feb 2009

desired mechanical anharmonicities [49, 50]. Knowing the noise level and other experimental parameters is thus important for a reliable optimization. Notice that if we select the amplitude to obtain a given signal strength, going towards ever higher harmonics is not necessarily favorable. For example, if $d_{min} = 1nm$ and $d^{(i)} = 1nm$, imaging at the second harmonic with $5nm$ oscillation amplitude results in a similar image as $20nm$ oscillation amplitude at the third harmonic, except that the $FWHM$ is a ~ 10 percent smaller. As a coarse rule, second and third harmonic demodulation with amplitudes on the order of the apex radius seem promising.

For the geometry discussed here, the signal is mostly sensitive to the region close to the interface. *aSNOM* measurements sensitive to larger depths have been observed [51]. The structures imaged in that work were significantly bigger than in the present study, which adds further phenomena such as a modified substrate reflectivity [52, 53]. Larger apex radii could equally increase the sensitivity to larger depths.

We have also illustrated limitations of small tip models for simulating typical experimental conditions. The obtained signal under such simplifications is considerably weaker and predicts an easier discrimination of the signature from the tip-inclusion interaction than appears possible in full tip models [14, 19]. Further, the central maximum for the small tips presents a much clearer asymmetry with respect to $x = 0$ than for the $500nm$ long tips. The asymmetry is introduced by the oblique illumination and the reduction for long tips could be due to the additional symmetry introduced by their axis [40]. Last, a better $FWHM$ is observed for the short tips, which points to a more spatially confined interaction [54] and reminds of the larger field confinement for isolated tips [40].

In summary, we have been able to simulate the phase and amplitude imaging process for *aSNOM*, including long tips and high harmonic demodulation, and shown the limitations of small tip models. The signal demonstrates subsurface imaging of small metallic particles if they are situated at nanometer distance to the interface. The signature of such inclusions is clear and strongly localized on the order of the structure size. The scanning conditions affect the obtained images, and higher harmonic demodulation, amplitudes on the order of the tip radius, scanning close to the sample and perfectly harmonic oscillation all seem favorable. Extending the present work to different substrates and tips will be helpful to guide experimental work and image interpretation by direct comparison between theory and measurements.

#104783 - $15.00 USD Received 1 Dec 2008; revised 14 Dec 2008; accepted 15 Dec 2008; published 6 Feb 2009